THE ASTROPHYSICAL JOURNAL, 482:186–202, 1997 June 10

HIGH-DENSITY, COMPACT H II REGIONS IN THE STARBURST GALAXIES NGC 3628 AND IC 694: HIGH-RESOLUTION VLA OBSERVATIONS OF THE H92α RADIO RECOMBINATION LINE

JUN-HUI ZHAO
Institute of Astronomy and Astrophysics, Academia Sinica, P.O. Box 1-87, Taipei, Taiwan 115;
Harvard-Smithsonian Center for Astrophysics, 60 Garden Street, MS 78, Cambridge, MA 02138

K. R. ANANTHARAMAIAH
Raman Research Institute, Bangalore 560 080, India

W. M. GOSS
National Radio Astronomy Observatory, P.O. Box O, Socorro NM 87801, USA

AND

F. VIALLEFOND
DEMIRM, Observatoire de Paris, 61 av. de l'Observatoire, F-75014 Paris, France
Received 1996 October 3; accepted 1996 December 12

ABSTRACT

Using the Very Large Array (VLA),[1] we have observed the H92α line in the nuclear regions of NGC 3628 and Arp 299 (IC 694 + NGC 3690) with an angular resolution of 1″. The radio recombination lines could provide quite important constraints to the physical conditions for the ionized gas in the nuclear regions. For the central nuclear components in NGC 3628, IC 694, and NGC 3690, we find that the electron density of the ionized gas is in the range 5×10^2 to 5×10^4 cm^{-3}, with corresponding geometrical sizes ranging from 25 to 0.01 pc. For the regions with a large line-to-continuum ratio, such as the anomalous kinematic components in IC 694 and NGC 3628, the electron density of the H II regions is well constrained. The derived parameters suggest the existence of ~100 high-density, compact H II regions ($n_e \sim 10^4$ cm^{-3} and $l \sim$ 1–2 pc) in these two components. The large number of high-density, compact H II regions deduced for these components can be regarded as evidence for enhanced massive star formation in anomalous kinematic structures that are often produced in interacting systems.

Our new H92α line observations reveal the presence of rotating circumnuclear ionized gas disks in both NGC 3628 and IC 694. From the analysis of the nuclear kinematics, we find that a total dynamical mass of 3×10^8 $M_\odot$ exists within a radius $R = 120$ pc in NGC 3628 and 7×10^8 $M_\odot$ within $R = 200$ pc in IC 694. The kinematics of the ionized gas and the models with a collection of H II regions infer that the ratio of H II to dynamical mass in the starburst nuclei varies from 1×10^{-4} (for the high-density, compact H II region model) to 1×10^{-2} (for the low-density, large H II region model).

Subject headings: galaxies: individual (NGC 3628, IC 694) — galaxies: ISM — galaxies: kinematics and dynamics — galaxies: starburst — radio lines: galaxies

1. INTRODUCTION

Over the past decade, both the sensitivity and spectral dynamic range of radio interferometers, such as the VLA, have been greatly improved. These improvements have resulted in several new breakthroughs in searching for extragalactic radio recombination lines (RRL; e.g., Anantharamaiah et al. 1993, hereafter AZGV; & Zhao et al. 1996, hereafter ZAGV) since the early detections toward M82 and NGC 253 (Shaver et al. 1977; Seaquist & Bell 1977). Recent detections of the H92α line from the starburst nuclei NGC 3628, IC 694, NGC 1365, Arp 220, NGC 2146, and M83 (AZGV; ZAGV) show a promising future for studying extragalactic RRLs with the VLA. Starburst galaxies are gas-rich systems and appear to be excellent targets for extragalactic RRL searches. To date, all the detected extragalactic RRLs (beyond the Magellanic Clouds) are associated with starburst nuclei. It has been demonstrated that observations of RRLs and modeling of the line emission (Puxley et al. 1991; AZGV; Seaquist, Kerton, & Bell 1994; ZAGV) are useful tools in studying the physical conditions of the ionized gas in extragalactic nuclei. Based on the previous detections and model calculations (see AZGV; ZAGV), the observed H92α line suggests that a large number of H II regions exist in these starburst nuclei. ZAGV showed the presence of a significant excess in the H92α intensity compared to the LTE values derived from Brα observations in the near-IR band for most starburst galaxies, suggesting that non-LTE effects are important. Also, a good correlation between the luminosities of the H92α and tracers of dense molecular gas (HCN and HCO^+) is found for these RRL nuclei. The RRL data can be compared with high-resolution observations of dense molecular gas, which will be important for studying the detailed star formation process in the starburst systems. Observations with high angular resolutions and at multiple RRL transitions will allow a determination of electron-density distribution in the starburst nuclear regions.

Furthermore, since the radio lines are not affected by extinction from dust, interferometric observations of RRLs

[1] The VLA is operated by the National Radio Astronomy Observatory (NRAO). The NRAO is a facility of the National Science Foundation operated under cooperative agreement by Associated Universities, Inc.

can reveal the kinematics in the central regions (<500 pc) for nearby galaxies with an angular resolution of $\sim 1''$. The central kinematics provide useful information to assess the mass content and dynamics in the nuclear regions (e.g., AZGV; Anantharamaiah & Goss 1996).

In this paper, we present high-resolution observations of the H92α recombination line from the nuclear regions of the starburst galaxies NGC 3628 and IC 694. Both NGC 3628 and IC 694 are located within the well-known interacting systems Leo Triplet and Arp 299, respectively. An H I emission tail in length of 45′ associated with NGC 3628, along with an H I bridge connecting NGC 3628 to NGC 3627, was observed by Rots (1978) and Haynes, Giovanelli, & Roberts (1979). The large-scale H I emission structure suggests that the gas surrounding the galaxies is substantially disturbed by the interaction. The complex structure in Arp 299 observed in radio and IR (e.g., Gehrz, Sramek, & Weedman 1983) could be understood as a consequence of NGC 3690 merging into IC 694 (Telesco, Decher, & Gatley 1985). The starburst activity in the nuclear regions of both NGC 3628 and IC 694 is plausibly a result of violent dynamical interactions (e.g., Larson & Tinsley 1978). The H92α lines from NGC 3628 and IC 694 were first detected by AZGV with a relatively high intensity among the galaxies that we have searched (ZAGV).

The paper is organized as follows. Section 2 summarizes the observations and data reduction. The results from the observations are presented in § 3. The nature of RRL emission regions and their astrophysical implications are discussed in § 4. Conclusions are presented in § 5. Finally, a discussion of a model with a collection of H II regions and a detailed procedure for deriving physical and geometrical parameters for nuclear H II regions are presented in the Appendix. $H_0 = 75$ km s^{-1} Mpc^{-1} is assumed.

2. OBSERVATIONS AND DATA REDUCTION

The H92α lines from the galaxies NGC 3628 and IC 694/NGC 3690 were detected in previous observations using the VLA in the C configuration (AZGV). During 1993 March, we observed these two galaxies in the H92α line using the VLA in the B configuration with an angular resolution of $\sim 1''$. The rest frequency of the H92α line is 8309.384 MHz. In all the observations, a VLA spectral line mode with 16 channels was used covering a bandwidth of 25 MHz, or a velocity coverage of ~ 900 km s^{-1}. The frequency resolution was 1.56 MHz (or 57 km s^{-1}). The correlator setup was identical to that used in the C array observations. Each source was observed for about 7 h. The observing parameters are summarized in Table 1. Columns (1)–(3) give the names and positions of the galaxies, respectively. The heliocentric velocity defined as $V_{\rm Hel} = (\lambda - \lambda_0)/\lambda_0\, c$ is given in column (4), where λ is the redshifted wavelength and λ_0 is the rest wavelength of the H92α line. Columns (5) and (6) list the calibrations used to correct the complex gains of the VLA system and to determine the frequency response (bandpass) of the instrument. The date of the observation is given in column (7), and the configuration in column (8). The flux density scale of the observations was set by using the radio source 3C 286. On-line Hanning smoothing was applied.

After initial calibrations, the visibility data obtained from the B and C arrays were combined. Further phase corrections for the continuum data were obtained using a self-calibration procedure. These phase corrections were also applied to each of the line channels. Continuum emission was subtracted utilizing the UVLIN algorithm (Cornwell, Uson, & Haddad 1992). Line images were made using natural weighting of the visibilities in order to achieve optimal sensitivity. The final rms noise in each of the channel images is typically 70 μJy beam^{-1}. For comparison, the rms noise in the observations (AZGV; ZAGV) was ~ 100 μJy beam^{-1}.

3. RESULTS

3.1. NGC 3628

3.1.1. *Distribution of Continuum Emission*

NGC 3628 is a member of the well-known interacting group the Leo Triplet. The H92α line was first detected in this galaxy by AZGV. The inferred distance is 11.5 Mpc, which implies a conversion from angular to linear scale of ≈ 50 pc arcsec^{-1}. A cleaned, uniformly weighted continuum image is presented in Figure 1. This image reveals the structure of the nuclear source with two continuum peaks separated by 3″, which were resolved into a number of compact components in earlier high-resolution images at 2 and 6 cm (Carral, Turner, & Ho 1990; Condon et al. 1982). Figure 2*a* (Plate 4) shows a naturally weighted continuum image of the central $12'' \times 16''$ region with a resolution of $1''.8 \times 1''.5$.

3.1.2. *Distribution of Line Intensity and Velocity Field*

Figures 2*b* and 2*c* (Plates 5 and 6) show the distribution of the integrated line intensity and the intensity-weighted velocity field. These images were obtained using a line data cube made by applying natural weight to the measured visibilities. The cutoff in each channel image used for making these moment images is $2\,\sigma$ ($1\,\sigma = 70$ mJy beam^{-1}). The angular resolution is $1''.8 \times 1''.5$ (P.A. $= -58°$). In general, the distribution of line emission is asymmetric about the major axis of the elongated continuum structure. Most of the line emission is concentrated in the nucleus with two anomalous RRL emission components (northwest [NW] and southeast [SE]) lying on either side of the nucleus (see Fig. 3). The line emission peaks at a velocity $V_{\rm Hel} = 840$ km s^{-1} are coincident with the continuum emission peak. The secondary peak of the continuum

TABLE 1

LOG OF OBSERVATIONS WITH THE VLA

Galaxy (1)	α (1950) (h m s) (2)	δ (1950) (° ′ ″) (3)	$V_{\rm Hel}$[a] (km s^{-1}) (4)	Calibrator (5)	BP Calibrator (6)	Observation Date (7)	Configuration (8)
NGC 3628	11 17 40.00	13 51 46.0	847	1119+183	3C 286/3C 84	1993 Mar 23	B
IC 694/NGC 3690.....	11 25 44.20	58 50 23.0	3132	1216+487/1053+704	3C 286/3C 84	1993 Mar 23	B

[a] $V_{\rm Hel} = (\lambda - \lambda_0/\lambda_0)c$, where c is the speed of light.

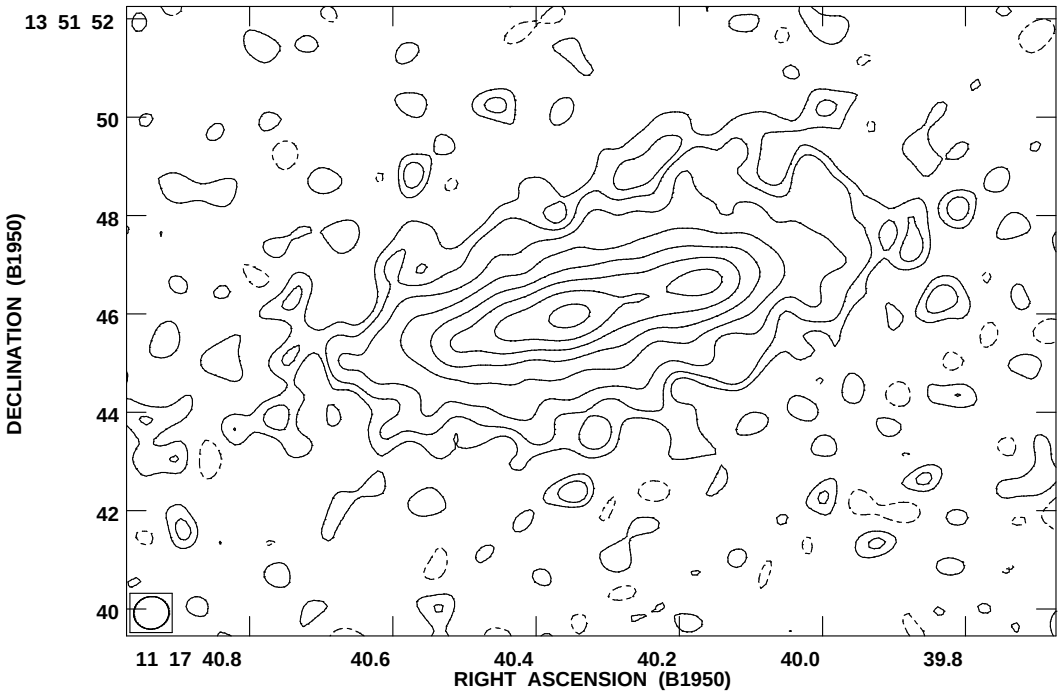

FIG. 1.—A uniformly weighted continuum image of the nuclear region in NGC 3628 observed at 8.3 GHz with the VLA. The beam is 0.″72 × 0.″66 (P.A. = −79°). The contours are −0.09, 0.06, 0.12, 0.24, 0.48, 0.96, 1.92, 3.84, 7.60 mJy beam^{-1}.

emission at about 3″ northwest of the nucleus is associated with a blueshifted H92α peak (NW component) at 710 km s^{-1}. This (NW) RRL component is associated with an anomalous molecular feature seen in H_2CO absorption (Baan & Goss 1992). The SE component at 900 km s^{-1} is extended and is composed of a filamentary structure with a peculiar velocity of V_{Hel} = 870 km s^{-1}. This kinematic component may be associated with the disturbed

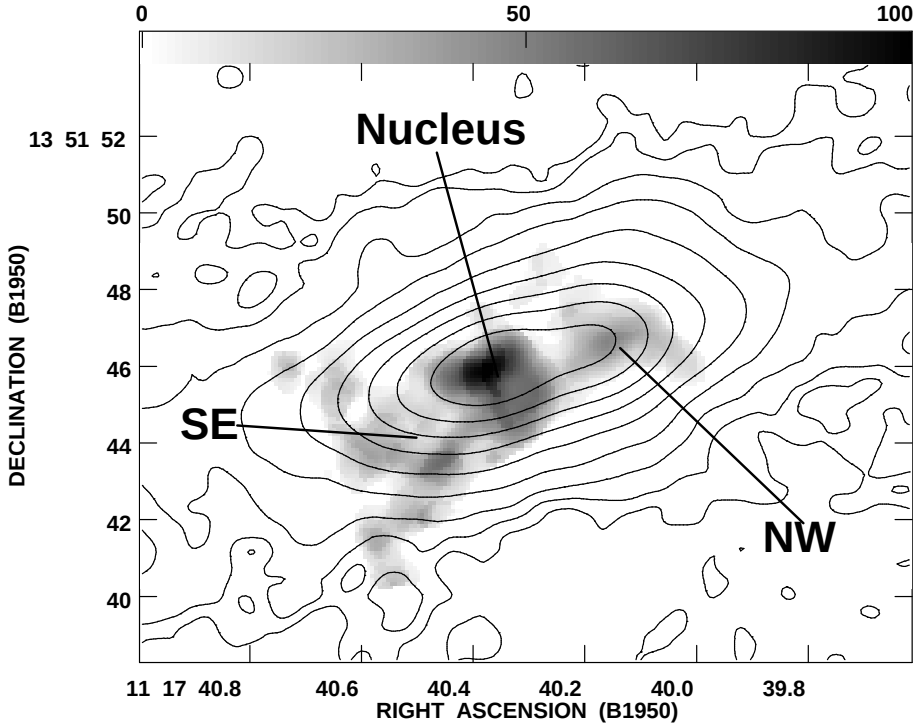

FIG. 3.—Integrated H92α line flux image of the nuclear region of NGC 3628. The gray-scale range is 0–100 mJy beam^{-1} km s^{-1}. The contours represent the continuum flux density levels from 0.04, 0.08, 0.16, 0.32, ..., 10.3 mJy beam^{-1}. The FWHP beam width for both line and continuum maps is 1.″8 × 1.″5 (P.A. = −58°). Three RRL emission components, Nucleus, SE, and NW, are labeled.

kinematic structure observed on a larger scale in both RRL and H I. The ionized component extends along the major axis of the galaxy up to 15″ southeast of the nucleus (see AZGV). The H I feature (plume or tail) extends to 45′ east of the galaxy (Rots 1978; Haynes et al. 1979).

The measured quantities, such as the total H92α line flux ($S_{\rm H92\alpha}\Delta V_{\rm FWHM}$), the continuum flux density ($S_{8.3\ \rm GHz}$), the emission area, the central heliocentric velocity, and the FWHM line width, are given for each component in Table 2.

3.1.3. *Distributions of Line-to-Continuum Ratio*

The line-to-continuum ($\int S_L\,dv/S_C$ or L/C) ratio image, shown in Figure 4 (Plate 7), was obtained from the integrated line flux image (Fig. 2*b*) divided by the continuum image (Fig. 2*a*) with a cutoff at 4 σ. An L/C ratio gradient is clearly present in the nuclear region. In the SE component, the L/C values are greater than 10 km s^{-1}. The L/C values corresponding to the components labeled "Nucleus" and "NW" are 5 and 4 km s^{-1}, respectively. Since the L/C distribution is not uniform, stimulated emission in a uniform ionized screen in front of the nonthermal region can be ruled out. The regions with larger L/C ratios imply the existence of compact H II regions where the line can be highly amplified through non-LTE effects (see the Appendix).

3.1.4. *The Kinematics of the Central 10″*

Figure 5 shows the velocity-position diagram, made along the major axis of the galaxy with P.A. = 105°. In general, the velocity structure in the central 4″ is dominated by a large velocity gradient (50 km s^{-1} per arcsec). The two anomalous kinematic features have a velocity gradient less than 30 km s^{-1} per arcsec. A large line width (FWHM) of 230 km s^{-1} is observed in the SE component, while the NW component has a width of 180 km s^{-1}.

3.2. Arp 299 (IC 694/NGC 3690)

3.2.1. *Distribution of Continuum Emission and an Anonymous Compact Source*

IC 694 and NGC 3690 constitute the interacting system Arp 299. Figure 6 shows a high resolution (0.″8 × 0.″7) continuum image of the Arp 299 system at 8.3 GHz. The compact components A and B are identified with the nuclei of IC 694 and NGC 3690, respectively. Components C and C′ are located in the interaction region of the two galaxies. In addition to these previously known sources, an unusual point source (IC 694 − 1990) located 11.″2 southwest (SW) of the IC 694 nucleus was detected with a flux density of 1.8 mJy at 8.44 GHz on 1990 March 1 by Huang et al. (1990), suggesting that this is a transient source and likely to be a radio supernova. The flux densities determined from our observations at 8.2 GHz on 1990 October 20 and 1993 March 22 are 1.8 ± 0.1 and 2.2 ± 0.1 mJy, respectively. An increase in flux density of about 20% between the two epochs is significant at the level of 4 σ. In the image observed at 1.413 GHz using the VLA in the A array with an angular resolution of 2″ in 1980 November (Condon et al. 1982), a source at the position of the anonymous compact is observed with a peak flux density of ∼4 mJy. However, the source was not detected with the VLA A array in 1989 February with an upper limit of 1 mJy at 1.49 GHz (J. J. Condon 1996, private communication). Thus, the compact source appears to be more than 12 yr old and shows significant time variations. These radio properties suggest that this compact source could be a background quasi-stellar object (QSO). Because of the faint nature of the source and the lack of a simultaneously measured radio spectrum, the existing data are consistent with either a background QSO or radio supernova (SN) origin.

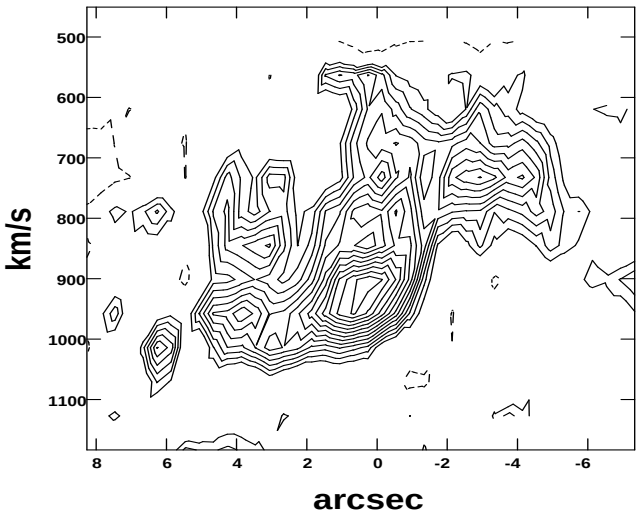

FIG. 5.—Velocity-position diagram of NGC 3628 taken along the major axis with a position angle of −75° (left to southeast and right to northwest). The reference position is $\alpha(1950) = 11^{\rm h}17^{\rm m}40^{\rm s}.14$, $\delta(1950) = -13°51'45''.2$. Contours are −0.8, 0.05, 0.08, 0.10, 0.13, 0.15, 0.18, 0.20, 0.23, 0.25, 0.28, 0.30, 0.33, 0.35 mJy beam^{-1}.

3.2.2. *Detection of the* H92α *Line in* NGC 3690

A detection of the H92α line from source A (IC 694) was reported by AZGV. Based on the combined B- and C-array data, the H92α line from the nuclear region of NGC 3690 (components B) at a central velocity of 3080 km s^{-1} is detected at a level of 3 σ. The velocity agrees with the H I absorption line of 3045 km s^{-1} (Baan & Haschick 1990). The H92α line spectrum of NGC 3690 is shown in Figure 7.

TABLE 2

MEASURED PARAMETERS FOR NGC 3628

Component (1)	$S_{\rm H92\alpha}\Delta V_{\rm FWHM}$ (mJy km s^{-1}) (2)	$S_{8.3\ \rm GHz}$ (mJy) (3)	Emission Area (beam) (4)	$V_{\rm Hel}$ (km s^{-1}) (5)	$\Delta V_{\rm FWHM}$ (km s^{-1}) (6)
NW	76 ± 5	20 ± 1	4.0 ± 0.5	710 ± 20	180 ± 15
Nucleus.....	150 ± 15	35 ± 2	3.8 ± 0.5	840 ± 40	290 ± 40
SE.....	161 ± 10	9.2 ± 0.5	6.2 ± 0.5	900 ± 30	230 ± 25

NOTE.—Beam (FWHM) = 1.″8 × 1.″5 (P.A. = −58°).

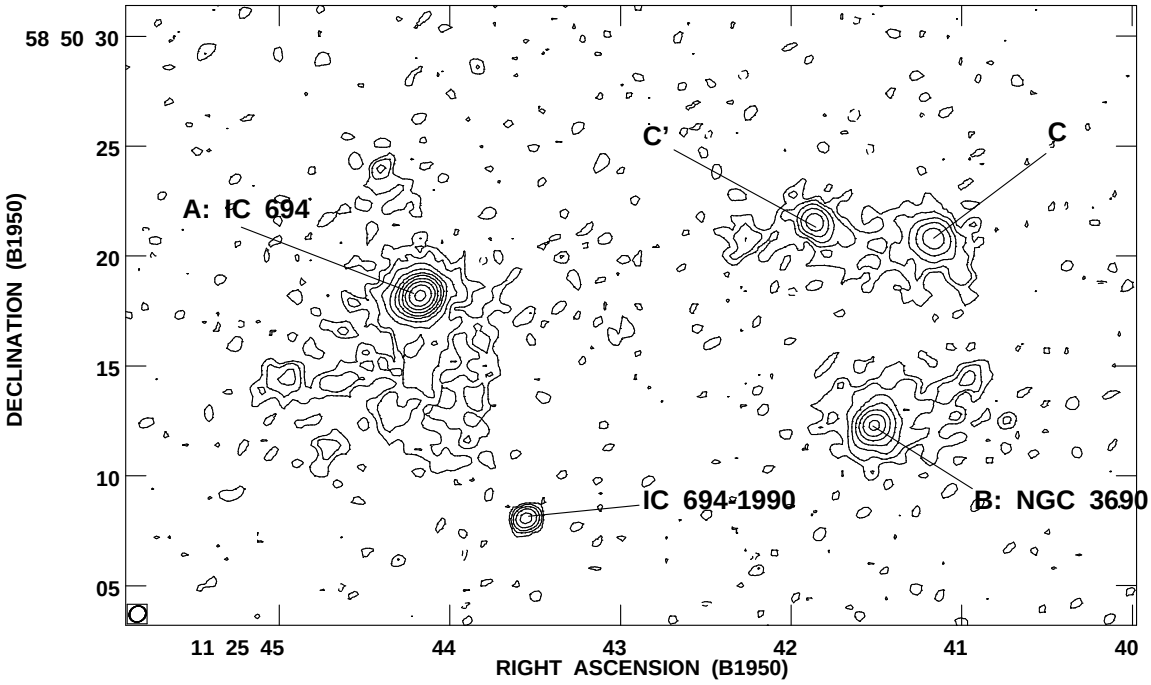

FIG. 6.—Continuum image of Arp 299 at 8.3 GHz made with uniform weighting. The contours are −0.15, 0.1, 0.2, 0.4, 0.8, 1.6, 3.2, 6.4, 12.8, 25.6, 51.2 mJy beam^{-1}. The beam size (FWHM) = 0.″8 × 0.″7 (P.A. = −54°).

No RRL detections were made toward the components C and C′.

3.2.3. *Distribution of Integrated Line Intensity and Nuclear Kinematics*

Figure 8 shows the distribution of integrated line intensity in the nuclear region of IC 694. Besides the compact nuclear emission, the high-resolution observations also reveal an elongated line emission structure to the SE of the nucleus. This extension is close to the major axis (P.A. ∼135°) of the continuum source (Baan & Haschick 1990). A weak extended CO emission (SE component) is also observed over a velocity range of (2956–3164 km s^{-1}) (Sargent & Scoville 1991).

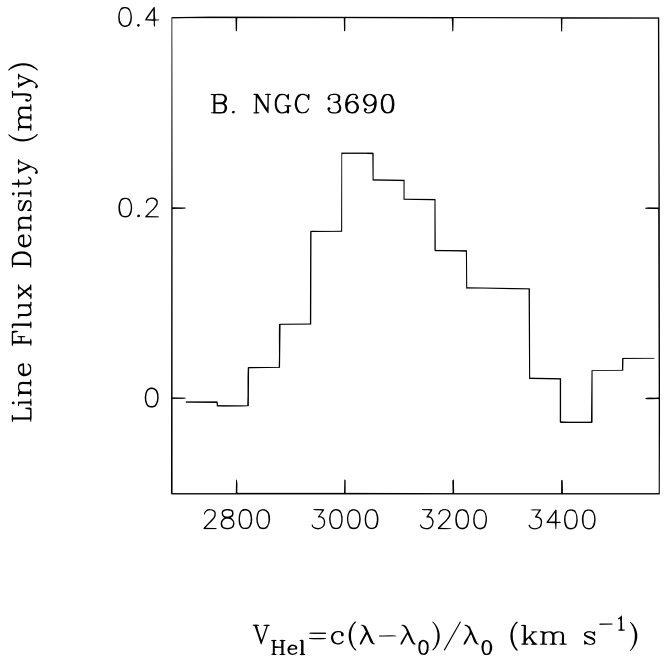

FIG. 7.—The H92α line spectrum detected toward the nucleus of NGC 3690.

Figure 9 shows the velocity-position diagram of IC 694. Two nuclear kinematic features are obvious. The main feature is characterized by a velocity gradient of 125 km s^{-1} per arcsec (or 1110 km s^{-1} kpc^{-1}) showing higher velocities in the NW region and lower velocities in the SE region. This kinematic structure may indicate the presence of a circumnuclear disk. Although the H92α emission peak is at a lower velocity (3000 km s^{-1}), the central velocity of 3110 km s^{-1} agrees with the nuclear H I disk centered at 3140 km s^{-1} (Baan & Haschick 1990).

In addition, an anomalous kinematic feature at a velocity of 3200 km s^{-1} is observed 2″ SE of the nucleus of IC 694 corresponding to the extended feature seen in the integrated line intensity image. The line width (FWHM) of this ionized component is about 250 km s^{-1}, which is larger than the molecular counterpart observed in CO of ∼100 km s^{-1} (Sargent & Scoville 1991).

3.2.4. *Distributions of Line-to-Continuum Ratio*

Figure 10 shows the line-to-continuum ratio ($\int S_L\,dv/S_C$) of IC 694; a large gradient of ∼3 km s^{-1} per arcsec is present along the major axis. The average value of $\int S_L\,dv/S_C$ for the nuclear component is ∼1 km s^{-1}, while the extended component has a larger line-to-continuum ratio (>10 km s^{-1}). Such a large L/C gradient across the nuclear region cannot be produced by a model with diffuse, low-density ionized gas and a stimulating background continuum source. The large L/C values in the SE region are

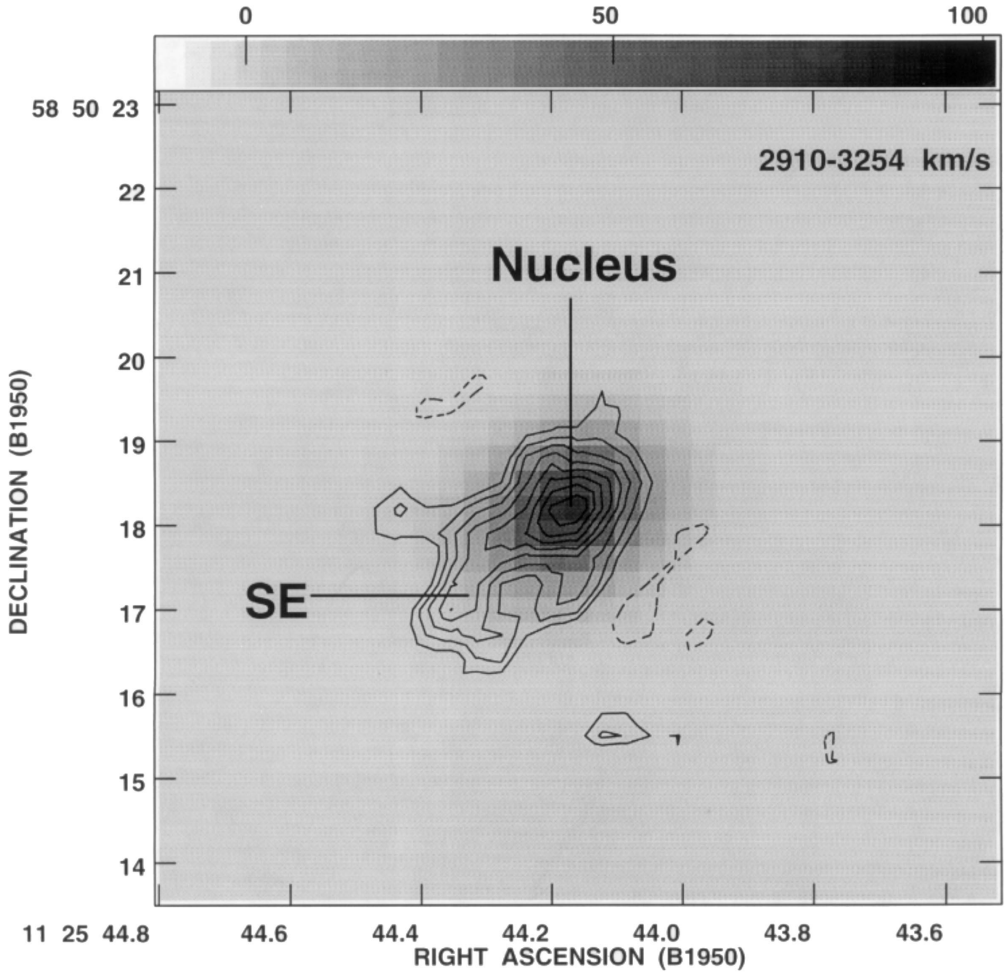

FIG. 8.—The H92α line emission of IC 694 integrated over the velocity range of 2910–3254 km s^{-1}. The contours are -30, 30, 40, 50, 60, 70, 80, 90, 100 mJy beam^{-1} km s^{-1}. The gray scale is -10–100 mJy beam^{-1}. The beam size (FWHM) is 0.″8 × 0.″7 (P.A. = $-54°$) for both the H92α line and the continuum. Both the nuclear component (Nucleus) and the southeast anomalous component (SE) are labeled.

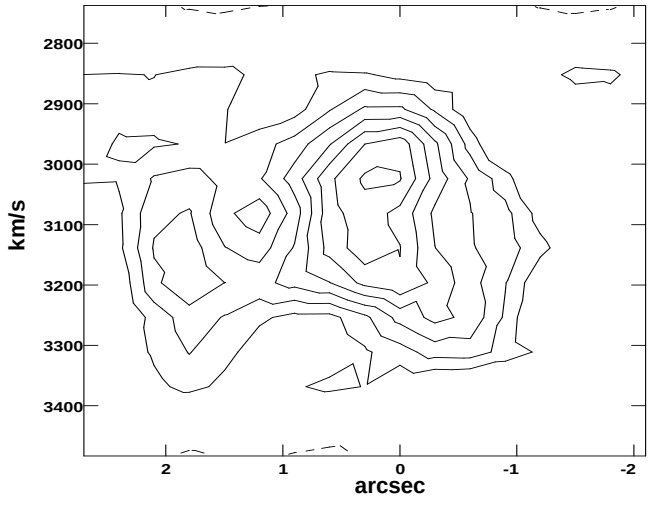

FIG. 9.—Velocity-position diagram of IC 694 taken along the major axis of the galaxy at P.A. = $-45°$. The reference position is $\alpha(1950) = 11^h25^m44^s.16$, $\delta(1950) = 58°50'18''.2$. Left is SE and right NW. The angular and velocity resolutions of this image are 0.″8 (*horizontal axis*) and 50 km s^{-1} (*vertical axis*), respectively.

important evidence for the hypothesis of a collection of compact H II regions that was proposed earlier (AZGV).

The measured quantities for the Arp 299 system are listed in Table 3.

4. INTERPRETATION AND DISCUSSION

4.1. *The Physical Conditions of the* H II *Regions in Starburst Nuclei*

A useful model, first discussed in AZGV for explaining the RRL emission from a starburst nuclear region, is based on a collection of compact H II regions produced by young massive stars formed during the starburst. This model suggests that the nonthermal radiation arising from a large number of supernova remnants gives rise to the continuum flux density at 3.5 cm (AZGV; ZAGV; and also see the Appendix). A number of free parameters (such as electron temperature [T_e], density [n_e], the geometrical size of the H II region [l], and the total number [N] of H II regions responsible for the RRL emission) must be determined in this model. The deduced physical quantities, such as the excitation parameter (U), the flux of ionizing photons, and the total H II mass, are sensitive to the selection of these free

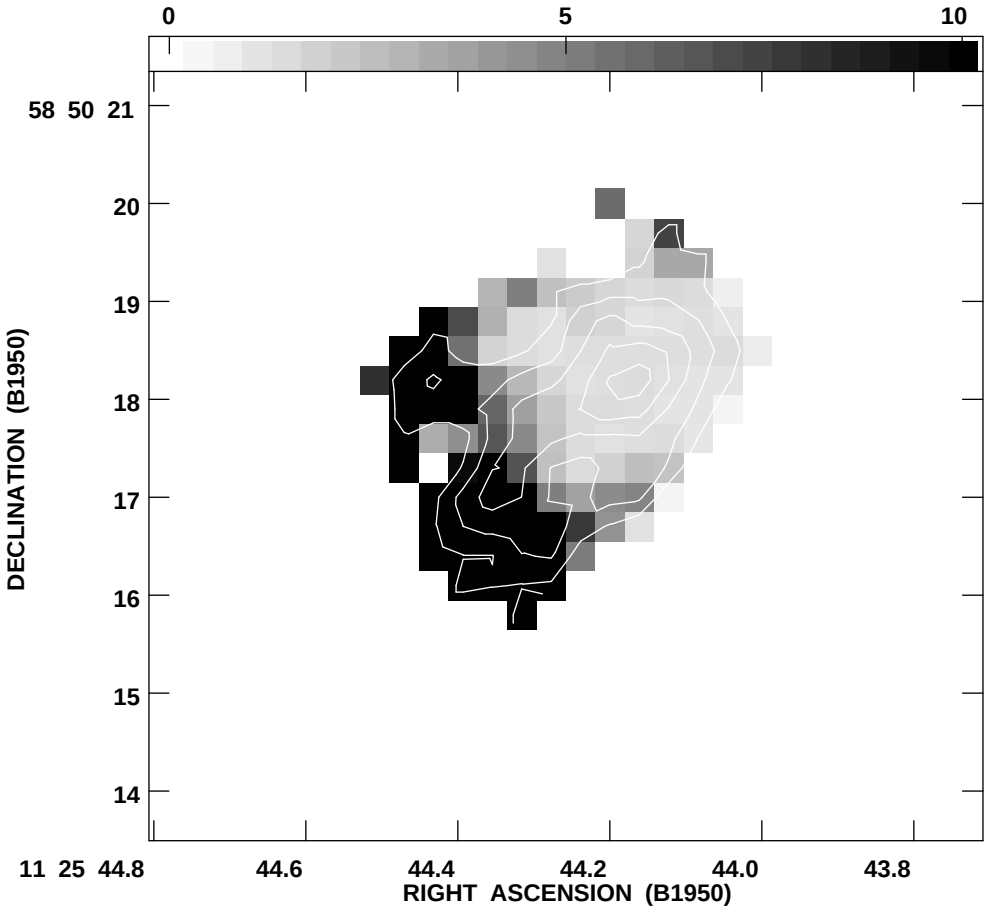

FIG. 10.—The line-to-continuum ratio ($\int S_{\mathrm{H92}\alpha}\,dv/S_{8.3\ \mathrm{GHz}}$, *gray scale*) image of IC 694 is overlaid on the integrated line flux image (*contours*). The gray scale indicates the ratio from 10 km s^{-1} (*black*) to 0 km s^{-1} (*white*). The contours are 20, 40, 60, 80, 100 mJy beam^{-1} km s^{-1}, the beam size (FWHM) is 0.″8 × 0.″7 (P.A. = −54°).

parameters. In principle, these parameters can be well constrained by high-resolution observations of several RRL transitions. However, the uncertainties of the parameters are substantial since observations exist only at a single line—the H92α line (AZGV; ZAGV). In the Appendix of this paper, we present a method for the analysis of RRL regions using a model with a collection of H II regions. We have shown in the Appendix that RRL observations can serve as a probe of density; i.e., for a specific electron density, there is a specific transition or frequency at which the line intensity is a maximum due to the non-LTE effect. In particular, we have shown that the line-to-continuum ratio, the free-free continuum flux density, the line width, and the angular size of the RRL emission region can effectively constrain the range of the mean excitation parameter of the constituent H II region. A detailed procedure for determining the free parameters is given in the Appendix. Employing this method for each of the RRL emission regions, we can derive the physical parameters of the H II regions that satisfy the observations.

In Table 4, we list the derived parameters. Column (1) is the name of the RRL emission region. Columns (2) and (3) are the free-free flux density (S_{FF}) and the ratio of the internal line flux to free-free flux density ($S_L^{\mathrm{int}}\Delta V_{\mathrm{obs}}/S_{FF}$). Columns (4)–(8) are the excitation parameter (U), optical depth (τ_C) at 8.3 GHz, electron density n_e, geometrical size (l), and rate of production of Lyman continuum photons (N_{Lyc}) of each H II region, respectively. Columns (9) and (10) are the total number of H II regions and the total H II mass in the RRL emission region. For columns (4)–(10), there are

TABLE 3

MEASURED PARAMETERS FOR ARP 299 SYSTEM

Component (1)	$S_{\mathrm{H92}\alpha}\Delta V_{\mathrm{FWHM}}$ (mJy km s^{-1}) (2)	$S_{8.3\ \mathrm{GHz}}$ (mJy) (3)	Emission Area (beam) (4)	V_{Hel} (km s^{-1}) (5)	ΔV_{FWHM} (km s^{-1}) (6)
IC 694:					
Nucleus.....	140 ± 15	77.6 ± 1	4.4 ± 0.5	3120 ± 50	380 ± 50
SE.....	105 ± 12	12.8 ± 0.5	4.6 ± 0.5	3200 ± 40	260 ± 35
NGC 3690					
Nucleus.....	55 ± 8	13 ± 0.5	2.6 ± 0.5	3080 ± 40	210 ± 30

NOTE.—Beam (FWHM) = 0.″8 × 0.″7 (P.A. = −53°).

TABLE 4

DEDUCED PHYSICAL PARAMETERS FOR THE H92α LINE REGIONS OBSERVED WITH THE VLA

Component (1)	S_{FF} (mJy) (2)	$S_L^{\rm int}\Delta V_{\rm obs}/S_{FF}$ (km s^{-1}) (3)	U (pc cm^{-2}) (4)	τ_C (8.4 GHz) (5)	n_e (10^4 cm^{-3}) (6)	l (pc) (7)	$N_{\rm Lyc}$ (10^{50} s^{-1}) (8)	N (9)	$M_{\rm H\,II}$ ($M_\odot$) (10)
NGC 3628: $T_e = 5000$ K, $\alpha = 1$, $\langle V_t\rangle = 10$ km s^{-1}, $D = 11.5$ Mpc									
NW	8.2	9.3	30	1.1	5	0.04	0.01	1.5×10^5	8×10^3
			430	0.08	0.1	8.5	40	34	3×10^5
Nucleus.....	14.4	10.4	32	1.8	6	0.01	0.01	3×10^5	1.6×10^4
			440	0.09	0.1	8.8	49	55	5×10^5
SE.....	3.9	43	280	2.0	1.5	0.9	12	120	2×10^4
			320	1.4	1.0	1.4	19	65	2×10^4
IC 694: $T_e = 5000$ K, $\alpha = 0.34$, $\langle V_t\rangle = 10$ km s^{-1}, $D = 40.3$ Mpc									
Nucleus.....	11.4	12.3	50	1.4	5	0.07	0.06	6.4×10^5	2×10^5
			820	0.06	0.05	25	590	79	9×10^6
SE.....	1.9	57	350	2.5	1.2	1.3	24	240	2×10^5
			560	0.83	0.5	3.8	130	42	2×10^5
NGC 3690: $T_e = 5000$ K, $\alpha = 0.8$, $\langle V_t\rangle = 10$ km s^{-1}, $D = 40.3$ Mpc									
Nucleus.....	4.1	14	60	1.7	5	0.09	0.01	1.5×10^5	6×10^4
			850	0.08	0.06	23	340	26	3×10^6

NOTE.—See text for explanation of rows for cols. (4)–(10).

two rows for each component that define a possible range of H II region parameters constrained by the H92α observations. The first row pertains to the highest possible density, compact H II region model with a corresponding lowest possible excitation parameter ($U_{\rm lower}$), while the second row pertains to the lowest possible density, large H II region model with the corresponding highest excitation parameter ($U_{\rm upper}$). Any model with a collection of H II regions satisfying the H92α line observations must fall within this range. In all the calculations, we assume the mean electron temperature $T_e = 5000$ K and the rms turbulent velocity is $\langle V_t\rangle = 10$ km s^{-1}.

4.1.1. NGC 3628

Based on the derived parameters, we calculate both the peak line and continuum flux densities for each of the H92α line components in NGC 3628. For the components associated with the Nucleus and the NW region, the ratio of the internal line flux to free-free continuum flux density is about 10 km s^{-1}, and the uncertainties in excitation parameter U are large, 30–450 pc cm^{-2}. Figures 11*a* and 11*b* illustrate the expected variation of the continuum and the peak flux density as a function of frequency for the high-density, compact (*solid line*) and the low-density, less compact (*dashed line*) H II region models. The peak line flux density from the low-density model is nearly constant in the frequency range 3–30 GHz, which is quite different from that of the high density model. The high-density model predicts a higher continuum flux density at high frequencies. Continuum observations at high frequency (such as 45 GHz with the VLA) would be useful to narrow the range of possible physical parameters. The contribution from stimulated emission due to the background nonthermal radiation is not significant in the nucleus of NGC 3628 [$S_L^{\rm stm}/(S_L^{\rm int} + S_L^{\rm stm}) < 10\%$ for larger and low-density H II region model and $< 0.5\%$ for the compact and high-density model; see the Appendix for the definitions of $S_L^{\rm int}$ and $S_L^{\rm stm}$].

A large line-to-continuum ratio ($S_L^{\rm int}\Delta V_{\rm HII}/S_{FF} = 43$) arises from the anomalous SE component. The physical parameters are well determined for this component. In this component, the presence of about 100 H II regions with excitation parameter $U = 300 \pm 20$ pc cm^{-2}, $l = 1.2 \pm 0.3$ pc, $n_e = 1.2 \pm 0.3 \times 10^4$ cm^{-3}, and $\tau_C = 1.7 \pm 0.3$ at 8.3 GHz are indicated by the observations. Each of the H II regions requires $N_{\rm Lyc} = 1.5 \times 10^{51}$ photons s^{-1}, which can be produced by $\sim$36 zero-age main-sequence (ZAMS) O5 stars. The total H II mass in the SE component is $\sim 2 \times 10^4\ M_\odot$. The peak line intensity as a function of frequency along with the continuum spectrum produced from this compact H II region model for the SE component is shown in Figure 11*c*. The maximum peak line flux density is predicted to be $\sim$2 mJy near 22 GHz (i.e., H66α). The continuum spectrum is flat for frequencies higher than 8 GHz. Stimulated emission due to the background nonthermal radiation can be neglected ($< 0.1\%$). The line emission is highly amplified because of a large non-LTE effect (the non-LTE factor is about 30; see the Appendix).

4.1.2. IC 694

The line-to-continuum ratio ($S_L^{\rm int}\Delta V_{\rm obs}/S_{FF}$) of 12 km s^{-1} was derived for the nuclear component in IC 694. A wide range of H II region parameters from $U = 50$ pc cm^{-2}, $\tau_C = 1.4$, $n_e = 5 \times 10^4$ cm^{-3}, $l = 0.06$ pc (corresponding to approximately a single ZAMS O7 star) to $U = 820$ pc cm^{-2}, $\tau_C = 0.06$, $n_e = 5 \times 10^2$ cm^{-3}, $l = 26$ pc ($\sim$1000 ZAMS O5 stars) are suggested by the models. For the lowest excitation parameter case, a total number of 6×10^5 compact H II regions is required for the nuclear component; if the excitation parameter is high, about 80 large ($l = 26$ pc), low-density ($n_e = 5 \times 10^2$ cm^{-3}) H II regions are required. In order to determine whether the compact and high-density or the large and lower-density H II regions contributes to the RRL emission in the nucleus, both higher- and lower-frequency observations are necessary. The lower-density H II region model ($l = 26$ pc, $n_e = 5 \times 10^2$ cm^{-3}) predicts that the line intensity reaches a maximum ($\sim$0.6 mJy) at a frequency near 4 GHz. The maximum intensity will shift to higher frequency if the density of the H II region is increased. For the model with the most compact H II regions ($n_e = 5 \times 10^4$ cm^{-3}, $l = 0.06$

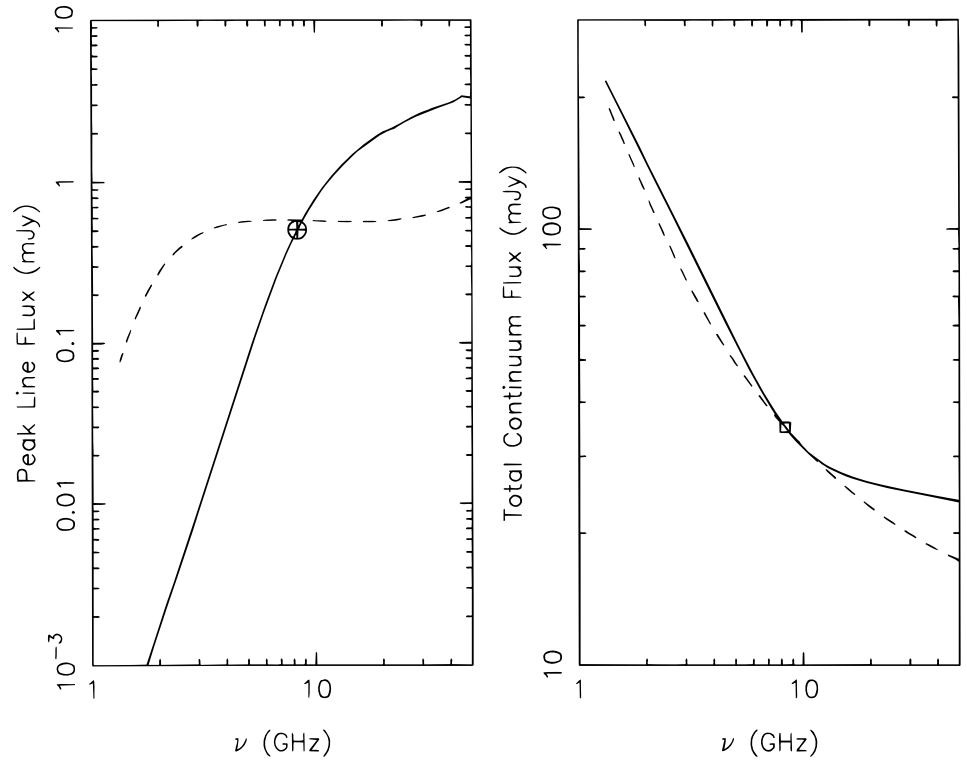

FIG. 11*a*

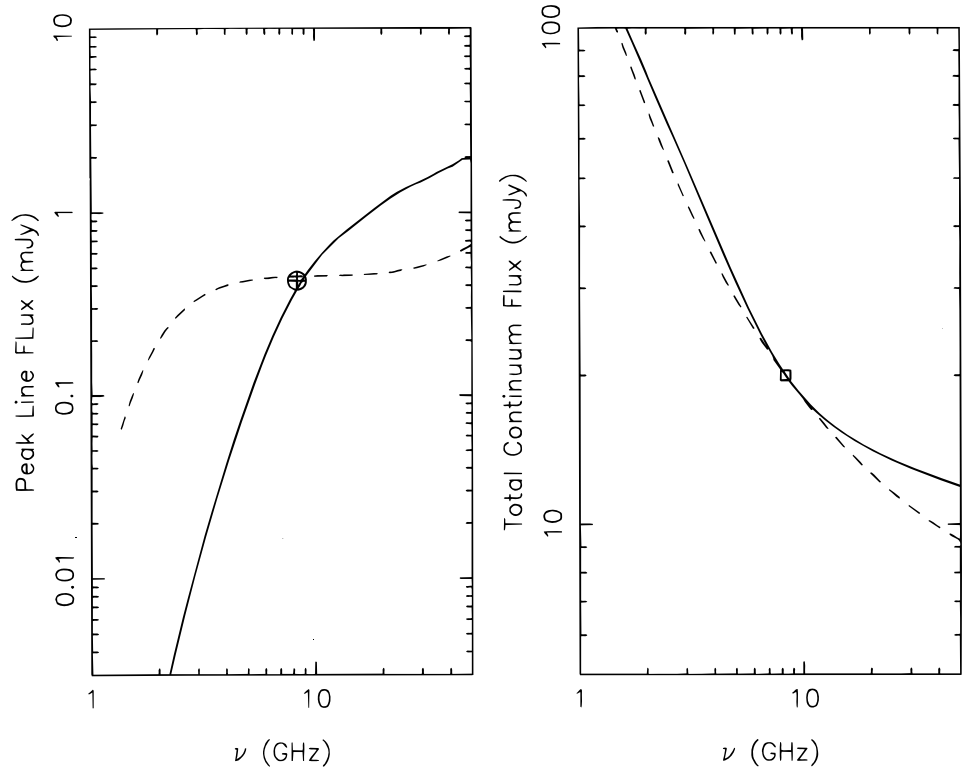

FIG. 11*b*

FIG. 11.—Plots of both line intensity and continuum flux density against frequency calculated for each RRL emission component in NGC 3628 based on the collective H II region model. The model curves are fitted to the observed H92α line (*circled cross*) and the 8.3 GHz continuum (*open square*). (*a*) The nuclear component (Nucleus): The solid curves represent a model with high-density, compact H II regions ($T_e = 5000$ K, $n_e = 5 \times 10^4$ cm^{-3}, $l = 0.07$ pc, $\langle V_t \rangle = 10$ km s^{-1}, $\alpha = 1$, $N = 5.5 \times 10^4$). The dashed curves correspond to a model with lower-density, larger H II regions ($T_e = 5000$ K, $n_e = 1 \times 10^3$ cm^{-3}, $l = 8.6$ pc, $\langle V_t \rangle = 10$ km s^{-1}, $\alpha = 1$, $N = 54$). (*b*) The anomalous component (NW): The solid curves represent a model with high-density, compact H II regions ($T_e = 5000$ K, $n_e = 5 \times 10^4$ cm^{-3}, $l = 0.04$ pc, $\langle V_t \rangle = 10$ km s^{-1}, $\alpha = 1$, $N = 1.2 \times 10^5$). The dashed curves correspond to a model with lower-density, larger H II regions ($T_e = 5000$ K, $n_e = 1 \times 10^3$ cm^{-3}, $l = 8$ pc, $\langle V_t \rangle = 10$ km s^{-1}, $\alpha = 1$, $N = 34$). (*c*) The anomalous component (SE): Only high-density, compact H II region models fit the observations. The solid curves correspond to a model with $T_e = 5000$ K, $n_e = 1 \times 10^4$ cm^{-3}, $l = 1.4$ pc, $\langle V_t \rangle = 10$ km s^{-1}, $\alpha = 1$, $N = 65$.

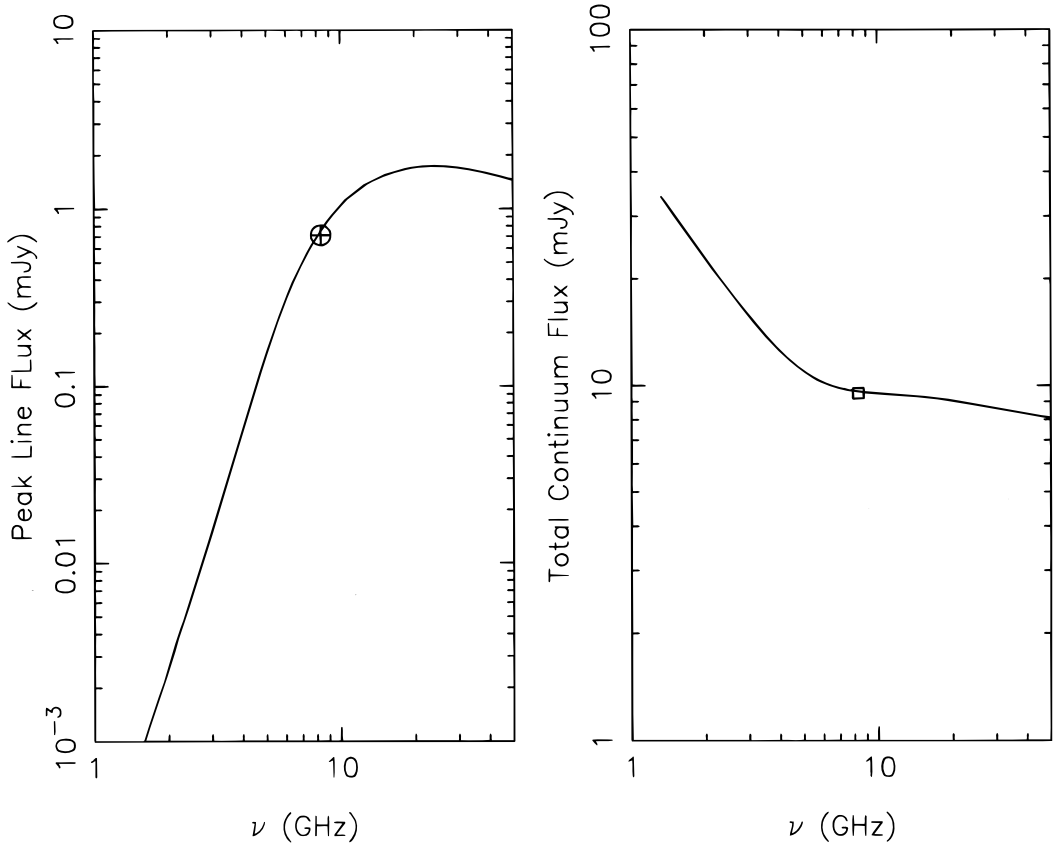

FIG. 11*c*

pc), higher line intensity (>2 mJy) at 45 GHz is predicted. We note that for the low-density model, the contribution from stimulated emission due to the background nonthermal emission is significant $[S_L^{\rm stm}/(S_L^{\rm int}+S_L^{\rm stm})\approx 40\%]$, while for the high-density model $S_L^{\rm stm}/(S_L^{\rm int}+S_L^{\rm stm})\approx 1\%$.

The SE component has the largest value of $S_L^{\rm int}\Delta V_{\rm obs}/S_{FF}=57$ km s^{-1} among the RRL emission regions in the galaxies presented in this paper. Our analysis suggests that the electron density of the H II regions within this component is in the range 5×10^3–1.2×10^4 cm^{-3} with corresponding sizes in the range 4–1 pc. An intermediate compact H II region model with $n_e=1\times10^4$ cm^{-3} and $l=1.6$ pc was used to illustrate both the continuum and line intensity as a function of frequency (see Fig. 12*b*). This model predicts a line intensity peak of 1 mJy near 22 GHz and a flat continuum spectrum at frequencies >10 GHz. No significant stimulated line emission due to the nonthermal background radiation contributes to the total line intensity of this component.

4.1.3. NGC 3690

Based on the H92α observations, our analysis shows that the nucleus of NGC 3690 has similar RRL properties as the nuclear components of IC 694 and NGC 3628. The line-to-continuum ratio ($S_L^{\rm int}\Delta V_{\rm H\,II}/S_{FF}$) is ~14 km s^{-1}, comparable to those observed in the IC 694 and NGC 3628 nuclei. Models with electron density in the range of 6×10^2–5×10^4 cm^{-3} can explain the observations. The corresponding linear sizes of the H II regions range from 20 to 0.1 pc. A total ionized mass of $6\times10^4\ M_\odot$ is required by the high-density model. The low-density model requires much larger H II mass ($3\times10^6\ M_\odot$) within the nucleus of NGC 3690. For the two extreme models, the predicted line and continuum intensities as a function of frequency are shown in Figure 13. The two models can be distinguished by making observations of other RRL transitions or radio continuum measurements at higher frequencies (>22 GHz).

4.2. *Local Enhancement in Massive Star Formation in the Interacting Systems*

Both NGC 3628 and IC 694 lie in interacting systems, i.e., Leo Triplet and Arp 299, respectively. Numerous molecular and H I observations show that several anomalous kinematic structures, such as NGC 3628-SE and IC 694-SE, may result from either a close encounter of a passing nearby galaxy (Leo Triplet; e.g., Rots 1978) or in a galaxy-galaxy merger (Arp 299; e.g., Larson & Tinsley 1978; Sargent & Scoville 1991). The current RRL observations and models show that there are a large number of compact H II regions in these interacting systems. We also observed that large line-to-continuum ratios are associated with the anomalous components NGC 3628-SE and IC 694-SE, which may be caused by a large amplification due to non-LTE effects in compact ($l\sim1$ pc) and high-density ($n_e\sim1\times10^4$ cm^{-3}) H II regions. The total H II masses associated with the anomalous components are $2\times10^4\ M_\odot$ in NGC 3628-SE and $2\times10^5\ M_\odot$ in IC 694-SE. The rates of production of Lyman continuum photons in NGC 3628-SE and IC 694-SE are 1.5×10^{53} and 6×10^{53} photons s^{-1}, corresponding to 3600 and 14,000 ZAMS O5 stars, respectively. These parameters suggest that local enhancement in massive star formation is associated with the anomalous kinematic components in these interacting systems. Thus, the RRL observations seem to favor the scenario that starburst activity may be triggered by mergers or galaxy-galaxy interactions (Telesco, Decher, & Gatley 1985; Sanders, Scoville, & Soifer 1991).

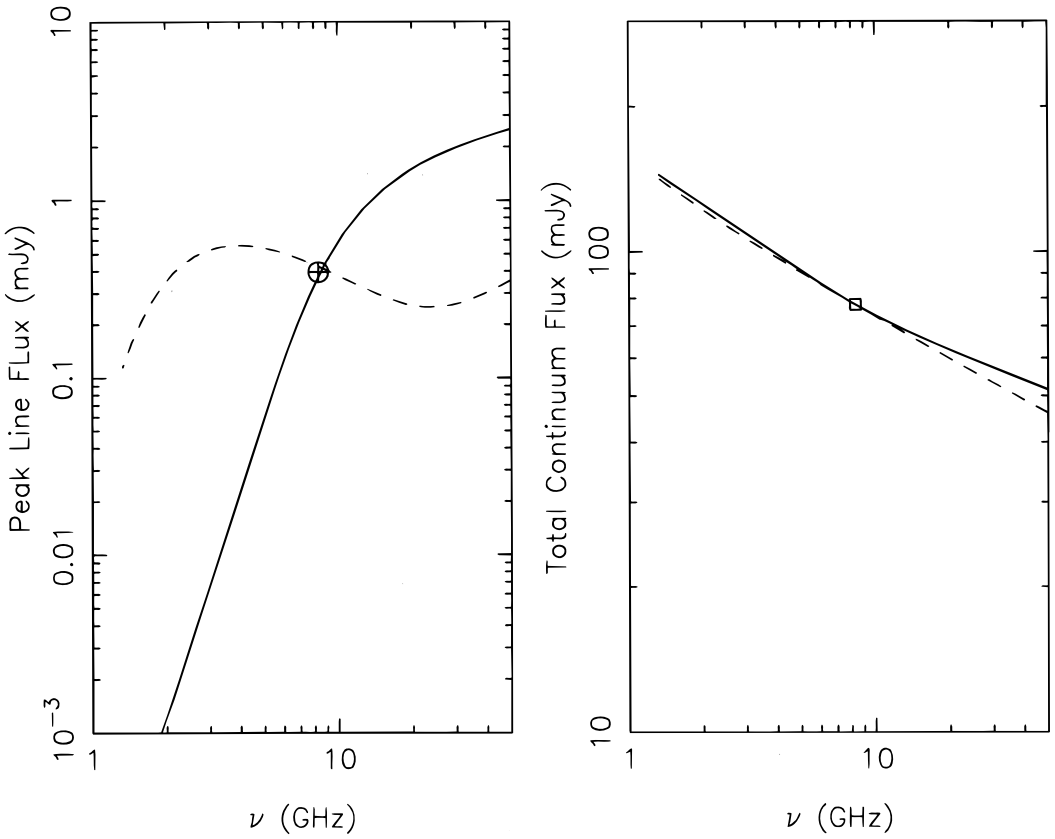

FIG. 12*a*

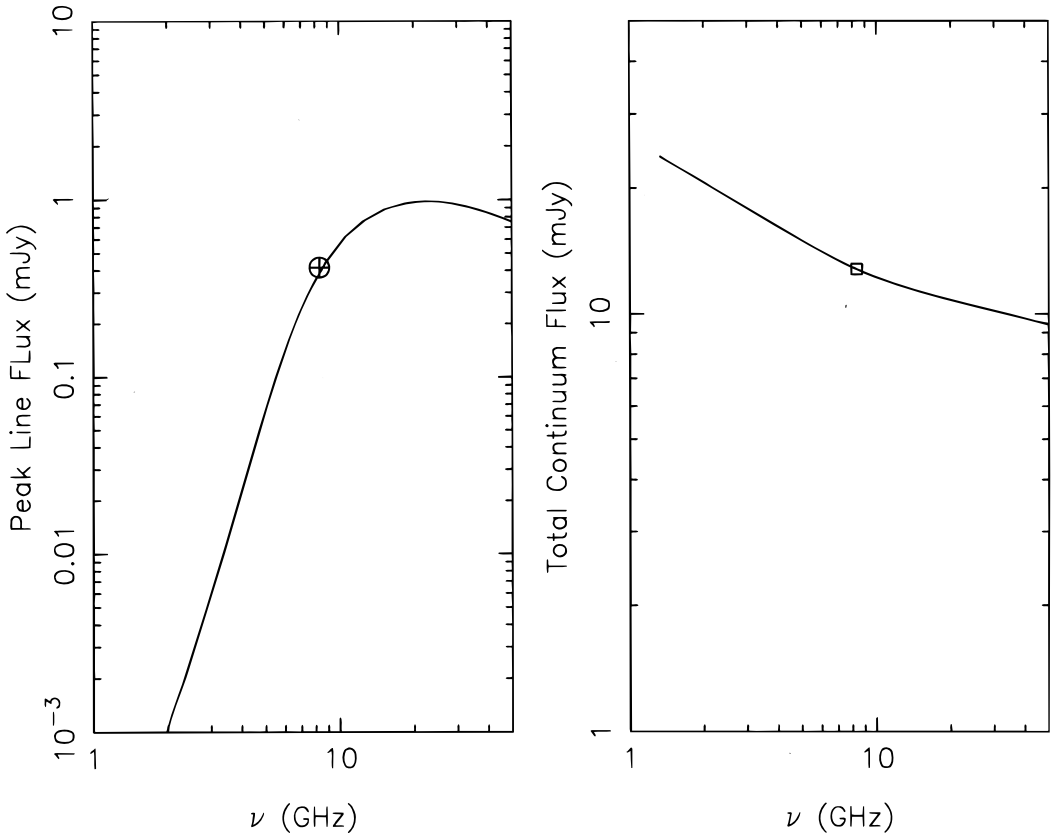

FIG. 12*b*

FIG. 12.—Plots of both line intensity and continuum flux density against frequency calculated for each RRL emission component in IC 694 based on the model with a collection of H II regions. The modeled curves are fitted with the observed H92a line (*circled cross*) and the 8.3 GHz continuum (*open square*). (*a*) The nuclear component (Nucleus): The solid curves represent a model with high-density, compact H II regions ($T_e = 5000$ K, $n_e = 5 \times 10^4$ cm^{-3}, $l = 0.07$ pc, $\langle V_t \rangle = 10$ km s^{-1}, $\alpha = 0.34$, $N = 6.3 \times 10^5$). The dashed curves correspond to a model with lower-density, larger H II regions ($T_e = 5000$ K, $n_e = 5 \times 10^2$ cm^{-3}, $l = 25$ pc, $\langle V_t \rangle = 10$ km s^{-1}, $\alpha = 0.34$, $N = 70$). (*b*) The anomalous component (SE): Only high-density, compact H II region models fit to the observations. The solid curves correspond to a model with $T_e = 5000$ K, $n_e = 1 \times 10^4$ cm^{-3}, $l = 1.6$ pc, $\langle V_t \rangle = 10$ km s^{-1}, $\alpha = 0.34$, $N = 390$.

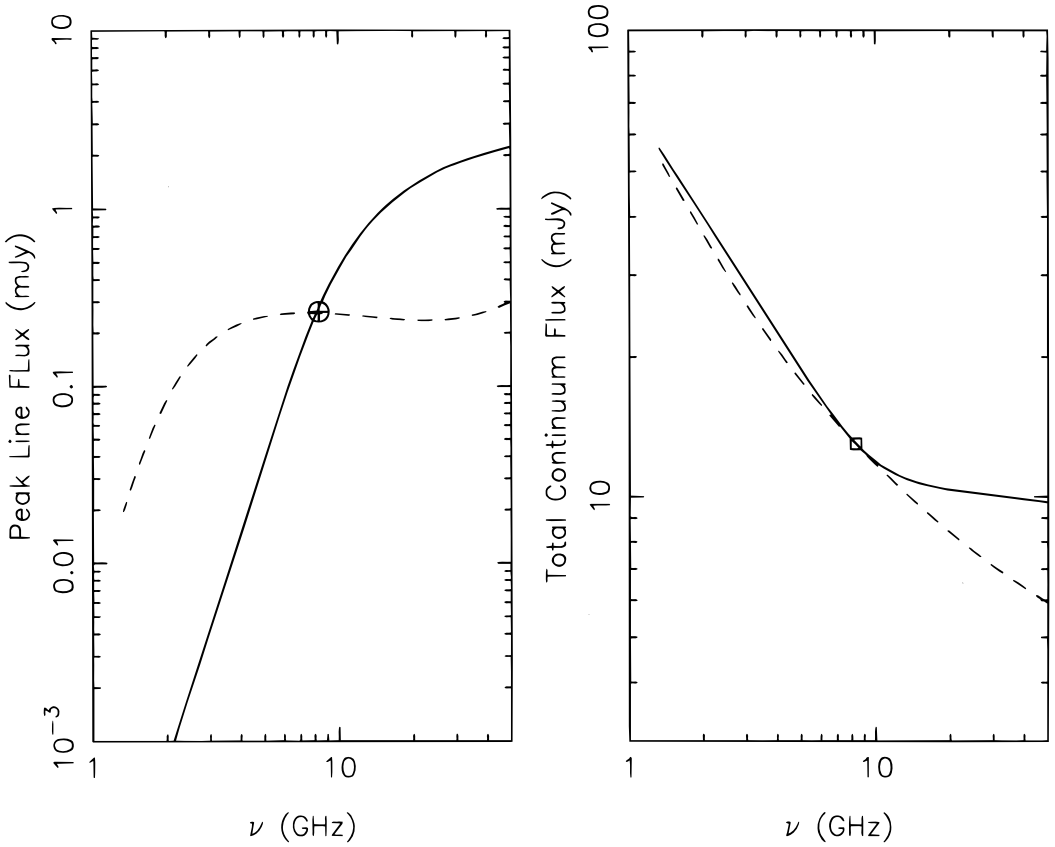

FIG. 13.—Plots of line intensity and continuum flux density against frequency calculated for each RRL emission component in NGC 3690 based on the model with a collection of H II regions. The model curves are fitted to the observed H92α line (*circled cross*) and the 8.3 GHz continuum (*open square*) data. The solid curves represent a model with high-density, compact H II regions ($T_e = 5000$ K, $n_e = 5 \times 10^4$ cm^{-3}, $l = 0.09$ pc, $\langle V_t \rangle = 10$ km s^{-1}, $\alpha = 0.8$, $N = 1.5 \times 10^5$). The dashed curves correspond to a model with lower-density, larger H II regions ($T_e = 5000$ K, $n_e = 1 \times 10^3$ cm^{-3}, $l = 11$ pc, $\langle V_t \rangle = 10$ km s^{-1}, $\alpha = 0.8$, $N = 85$).

4.3. *Circumnuclear Kinematics and Dynamical Mass*

The high angular resolution RRL observations presented here reveal a rotating circumnuclear disk (CND) in both galaxies, with an angular size of 4″ for NGC 3628 and 2″ for IC 694. In the case of an edge-on disk (an inclination $i = 90°$), both the maximum rotational velocity (V_r) and the radius of the rotating nuclear disk (R) can be determined. Thus the dynamical mass within the disk can be estimated using the relation (AZGV)

$$M_D = 2.3 \times 10^8 \, M_\odot \left(\frac{V_r}{100 \text{ km s}^{-1}} \right)^2 \left(\frac{R}{100 \text{ pc}} \right). \quad (1)$$

We infer total dynamical masses of $3 \times 10^8 \, M_\odot$ within the central radius of 120 pc of NGC 3628 and $7 \times 10^8 \, M_\odot$ within $R = 200$ pc of IC 694 (see Table 5). Both NGC 3628 ($i > 86°$; Boisse, Casoli, & Combes 1987) and IC 694 ($i \sim 70°$; Augarde & Lequeux 1985) are nearly edge-on. Assuming that the nuclear disks have similar inclinations, an inclination correction is not significant (e.g., if $i > 70°$, the dynamical mass would be underestimated by no more than 15%).

Since the inferred H II masses depend on the density and size of the individual H II regions within the nuclear regions, the ratio of ionized gas to dynamical mass ($M_{\rm H\,II}/M_D$) inferred from the various models is different. Based on the values of $M_{\rm H\,II}$ constrained by the H92α observations (Table 4), we find that in the nuclear region of NGC 3628, this ratio varies from 6×10^{-5} (for high-density, compact H II regions) to 2×10^{-3} (for low-density, large H II regions). In

TABLE 5

PARAMETERS FOR THE NUCLEI IN NGC 3628 AND IC 694

Parameters[a] (1)	NGC 3628 (2)	IC 694 (3)
Rotational velocity (km s^{-1})[a]	100	125
Radius of CND (pc)	120	200
Dynamic mass ($10^8 \, M_\odot$)	2.8	7.2
$M_{\rm H\,II}/M_D$	6×10^{-5} to 2×10^{-3}	3×10^{-4} to 1×10^{-2}

[a] Uncertainties of the two quantities (V_r and R) are ~20% of the mean values due to the limited velocity and spatial resolutions. Taking the uncertainties in V_r and R along with the uncertainty in inclination angles of the CNDs into account, the uncertainty in the dynamic mass is ~50%. The range of values ($M_{\rm H\,II}/M_D$) corresponds to the high-density, compact H II region and the low-density, large H II region models given in Table 4

IC 694, the value of $M_{\rm H\,II}/M_D$ varies from 3×10^{-4} to 1×10^{-2} with the corresponding high-density, compact H II region ($n_e = 5 \times 10^4$ cm^{-3}, $l = 0.1$) and low-density, large H II region ($n_e = 5 \times 10^2$ cm^{-3}, $l = 25$) models, respectively.

Let us also compare the mass content derived from these starburst nuclei with those inferred from the center of the giant elliptical galaxy M87. A massive black hole is believed to be harbored in the nucleus of this galaxy, which powers the energetic radio source Virgo A. Based on the *Hubble Space Telescope* observations, the central mass within the inner 0.″25 ($\sim$20 pc for $D = 15$ Mpc) is about $2.4 \times 10^9\ M_\odot$, while the inferred ionized mass of the nuclear disk in a size of 1″, or 80 pc, is $3.9 \times 10^3\ M_\odot$ (Ford et al. 1994; Harms et al. 1994). Assuming that the dynamical mass within the inner 1″ is dominated by this massive compact object, the ratio of ionized gas to the dynamical mass in the nuclear disk is $\sim 2 \times 10^{-6}$. This value is about 2 (3) orders in magnitude smaller than those derived from NGC 3628 and IC 694 using a high- (low-) density model. In addition, based on our RRL observations of NGC 3628, the inferred $3 \times 10^8\ M_\odot$ within a radius of 120 pc could not rule out the possibility that a massive black hole exists in the center. Both higher angular resolution and more sensitive observations are required in order to investigate further if the nuclear kinematics in NGC 3628 are produced by a small version of a black hole in comparison with that inferred from M87.

5. CONCLUSION

Using the VLA with an angular resolution of 1″ and a velocity resolution of 50 km s^{-1}, we have observed the starburst nuclei of NGC 3628, IC 694, and NGC 3690 in the interacting systems (Leo Triplet and Arp 299) using the H92α transition. We have shown that the RRL observations provide a useful tool for studying the physical conditions and kinematics of the ionized gas in the heavily obscured nuclear region of starburst galaxies.

Based on a model with a collection of H II regions, we have shown that physical parameters for the ionized gas can be constrained within a range from these observations. For the central nuclear components in NGC 3628, IC 694, and NGC 3690, we find that the electron density of the H II regions is in the range $n_e = 5 \times 10^2$–5×10^4 cm^{-3}, with corresponding geometrical sizes ranging from 25 to 0.01 pc. For the regions with large line-to-continuum ratios such as the anomalous components IC 694-SE and NGC 3628-SE, the physical conditions of the H II regions can be particularly well determined. The derived parameters suggest the existence of high-density, compact H II regions ($n_e = 1 \times 10^4$ cm^{-2} and $l = 1$–2 pc) in these two components (IC 694-SE and NGC 3628-SE). The high-density, compact H II regions inferred from the H92α line study favors the suggestion that local enhancements in the massive star formation may be associated with the anomalous kinematic components.

From the H92α line observations of the circumnuclear disks, we derive total dynamical masses of $2.8 \times 10^8\ M_\odot$ within the central 120 pc of NGC 3628 and $7.2 \times 10^8\ M_\odot$ within the central 200 pc of IC 694. Since the inferred ionized mass depends on the properties of the H II regions (electron density and size), we find that the ratio of ionized gas to dynamical mass is in the range 1×10^{-4} to 1×10^{-2} with the corresponding high-density, compact H II region and low-density, large H II region models, respectively.

J. H. Z. thanks the ASIAA for their hospitality. This research was supported in parts by NSC 85-2816-M001-006L of Taiwan. We thank Alan Roy for useful comments.

APPENDIX

MODEL FOR COLLECTION OF H II REGIONS

RRLs arising from the nuclear region of a starburst galaxy can be explained by a model with a collection of H II regions. This model was first proposed by a model with a collection of H II regions. This model was first proposed by Puxley et al. (1991) and further developed by AZGV. In the model proposed by AZGV, each of the H II regions is characterized by electron temperature (T_e), electron density (n_e), linear size (l), and turbulent velocity ($\langle V_t \rangle$). Using the H II region model, we present here a method for determining reliable physical and geometrical parameters of the H II regions based on the high angular resolution H92α line observations.

A1. A COLLECTION OF H II REGIONS

If the N H II regions lie within a uniformly distributed background continuum emitting region ($S_{\rm Cbg}$), the total continuum flux density S_{FF}, the internal peak line flux density $S_L^{\rm int}$, and the externally stimulated line flux $S_L^{\rm stm}$ are given by

$$S_{FF} = \frac{2kv^2}{c^2}\, N\Omega_{\rm H\,II}\, T_e(1 - e^{-\tau_C})\,, \tag{A1}$$

where the continuum optical depth $\tau_C = 8.235 \times 10^{-2}\alpha(v, T_e)n_e^2\, lT_e^{-1.35}\, \nu_{\rm GHz}^{-21}$; and $\Omega_{\rm H\,II}$ is the solid angle subtended by an individual H II region. Here $\alpha(v, T_e)$ is a dimensionless factor of order unity for the densities and temperatures under consideration.

$$S_L^{\rm int} = \frac{2kv^2}{c^2}\, N\Omega_{\rm H\,II}\, \frac{\Delta V_{\rm H\,II}}{\Delta V_{\rm obs}}\, T_e\left[\left(\frac{b_m\tau_L^* + \tau_C}{\tau_L + \tau_C}\right)(1 - e^{-(\tau_L + \tau_C)}) - (1 - e^{-\tau_C})\right] \tag{A2}$$

and

$$S_L^{\rm stm} = N^{1/3} f_{\rm H\,II}^{2/3}\left(\frac{\Delta V_{\rm H\,II}}{\Delta V_{\rm obs}}\right) S_{\rm Cbg}\, e^{-\tau_C}(e^{-\tau_L} - 1)\,, \tag{A3}$$

respectively. The total line flux density is $S_L = S_L^{\rm int} + S_L^{\rm stm}$. The central line optical depth is related to the LTE value (τ_L^*) through $\tau_L = b_n \beta_n \tau_L^*$, where b_n and β_n are the departure coefficients (e.g., Roelfsema & Goss 1992). Both b_n and β_n used in this paper were interpolated from the values given in Salem & Brockehurst (1979) and Walmsley (1990). The ratio $\Delta V_{\rm H\,II}/\Delta V_{\rm obs}$ accounts for the assumption that the observed line width may result from the individual H II regions being at different central velocities. These equations (A1A3) are only valid for small values of $N_{\rm H\,II}^{\rm los} \leq 1$, the average number of H II regions along any line of sight, which is given by

$$N_{\rm H\,II}^{\rm los} = N^{1/3} f_{\rm H\,II}^{2/3}\,, \tag{A4}$$

where $f_{\rm H\,II} = N(l/L)^3$ (the volume filling factor) and L is the linear size of the RRL emission region. No shadowing effects are taken into account. The effect of shadowing of one H II region by another is important only if $N_{\rm H\,II}^{\rm los} > 1$ and $\tau_C \geq 1$, which does not occur in any of the H II models considered for starburst nuclei (AZGV; ZAGV).

In addition, since $f_{\rm H\,II}$ in the line emitting regions is very small ($\sim 10^{-6}$), only a small fraction of background nonthermal radiation along the line of sight is intercepted by the H II regions. For compact H II regions ($n_e > 1 \times 10^3$ cm^{-3}), the contribution of stimulated line emission due to the background radiation at 8 GHz is only a few percent or less in a starburst nucleus (see AZGV; ZAGV).

We also define the non-LTE factor,

$$F_{\rm nLTE} \equiv \frac{S_L^{\rm int}}{S_L^{\rm int*}}\,, \tag{A5}$$

where the asterisk (*) denotes the LTE value. For small opacities,

$$F_{\rm nLTE} \approx b_n\left(\frac{1-\beta_n\tau_C}{2}\right). \tag{A6}$$

For large opacities,

$$F_{\rm nLTE} \approx b_n(1-\beta_n)\,\frac{\tau_L^*}{\tau_C}\,e^{\tau_C}\,. \tag{A7}$$

The non-LTE effect is important in an optically thick H II region.

A2. EXCITATION PARAMETER AND OBSERVATIONAL CONSTRAINTS

The excitation parameter describes the excitation and ionization properties of an ionized medium surrounding a star and is defined as

$$U = \frac{l}{2}\,n_e^{2/3} \qquad ({\rm pc\ cm^{-2}})\,, \tag{A8}$$

or $U^3 = 10 n_e M_{\rm H\,II}(M_\odot)$. The excitation parameter U can be understood as the radius of the Strömgren sphere for an H II region of electron density of 1 cm^{-3}. The flux of the Lyman continuum photons is proportional to U^3:

$$N_{\rm Lyc} = 5.0 \times 10^{46} T_e^{-0.8} U^3 \qquad ({\rm photons\ s^{-1}})\,. \tag{A9}$$

For a given excitation parameter U, the radiative properties of an H II region such as the optical depth and flux density of both the line and continuum are functions of density (n_e), temperature (T_e), and the linear size (l). In Figure A1, we numerically show these quantities for the H92α transition frequency as a function of electron density for $T_e = 5000$ K and various values of the excitation parameter U. For the H92α transition, the total optical depth has the highest negative value at $n_e \approx 6 \times 10^3$ cm^{-3} (see Fig. 14a). The peak line flux density reaches a maximum at n_e in a range from 1.5×10^4–6×10^3 cm^{-3}, corresponding to U from 100 to 1500 pc cm^{-2}, respectively (see Fig. 14b). Figure 14b shows that the non-LTE effect, in fact, provides an observational "filter" that selects a particular density regime where the line emission is highly enhanced.

In addition, the maximum value of $S_L^{\rm int}/S_{FF}$ is proportional to the excitation parameter U, which is an observable quantity that constrains the excitation parameter chosen in a particular model (see Fig. 14*d*). Figure 14*d* also shows that for a fixed excitation parameter U, the non-LTE factor ($F_{\rm nLTE}$) increases as the electron density increases.

In the model with a collection of H II regions, there are numerous free parameters, such as T_e, n_e, l, U, N (total number H II regions). These parameters can, in principle, be well constrained by multifrequency continuum and line observations. Other physical quantities such as H II mass and Lyman continuum flux can be deduced from the models. The flux densities of both line and continuum emissions, the size of the emission region, and the total line width can be directly determined from the observations. AZGV have discussed several physical constraints that can be applied during the model process to limit the range of possible parameters. Here we discuss an additional constraint that can be applied to the excitation parameter, U, of the H II regions. This constraint limits the range of densities and geometrical sizes of the H II regions based on the free-free continuum flux density that can be derived from the observations, the line width, and the line-to-continuum ratio.

A2.1. *Free-Free Continuum Flux Density, Line Width, and Upper Limit to Excitation Parameter*

We rewrite equation (A1) as

$$\left(\frac{S_{FF}}{\rm mJy}\right) = 15.9\left(\frac{U}{100\ {\rm pc\ cm^{-2}}}\right)^3 \frac{N}{D_{\rm Mpc}^2}\,\alpha(\nu,\,T_e)T_e^{-0.35}\left(\frac{1-e^{-\tau_C}}{\tau_C}\right)\nu_{\rm GHz}^{-0.1}\,, \tag{A10}$$

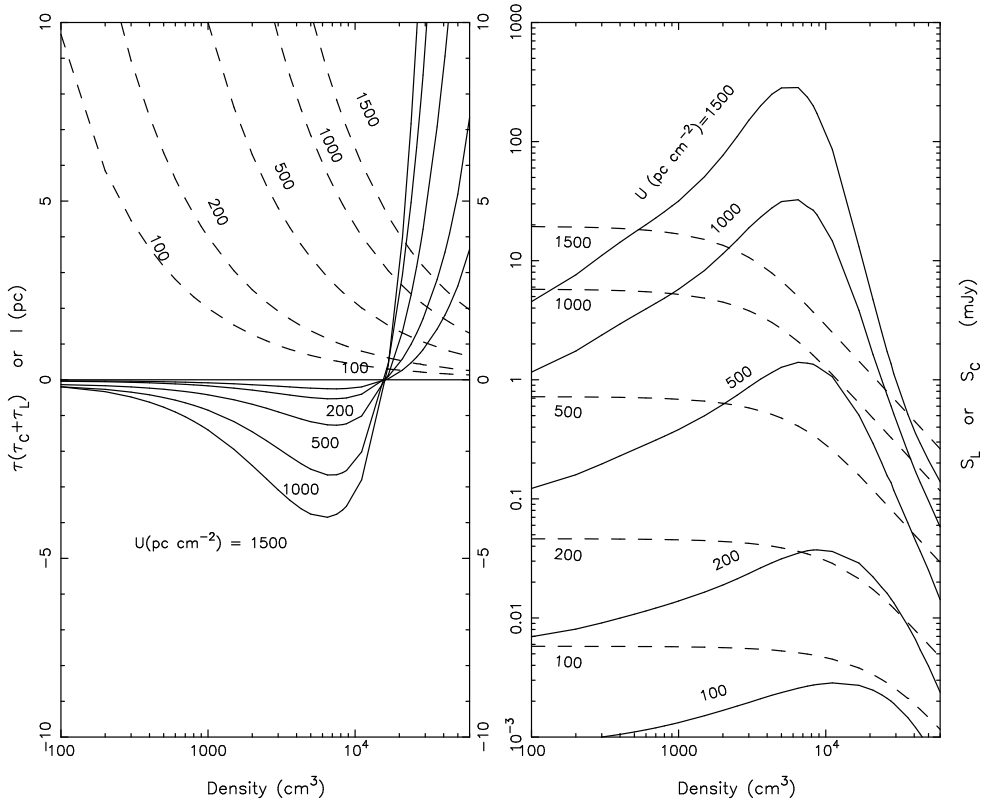

FIG. 14*a*

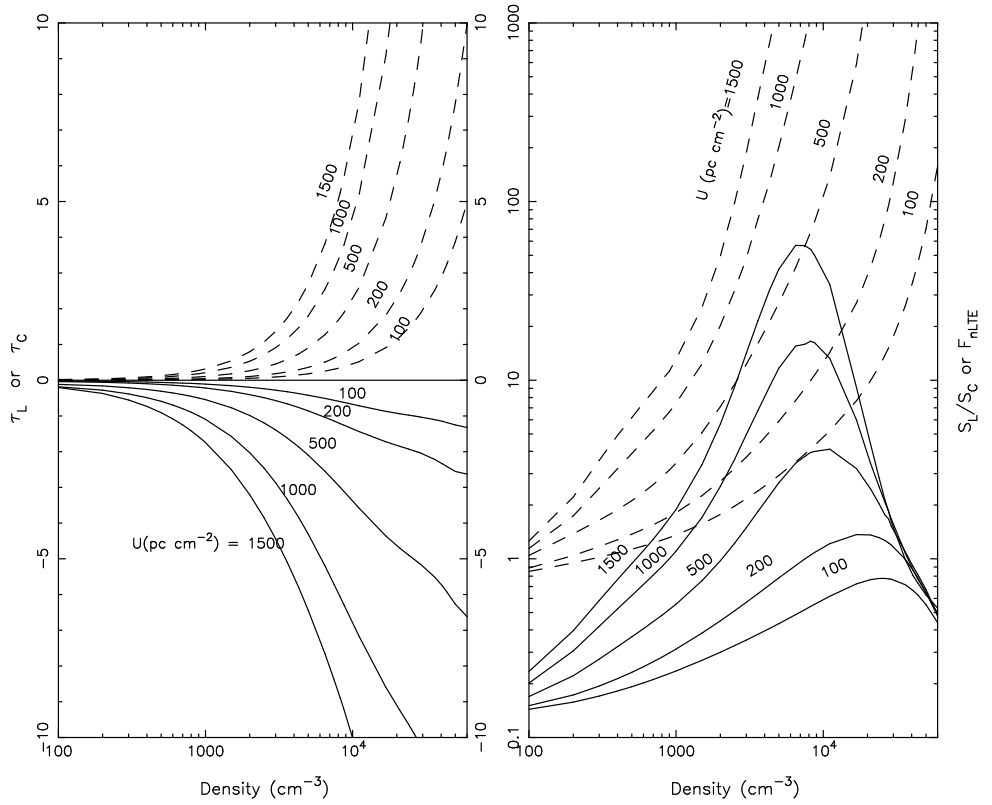

FIG. 14*b*

FIG. 14.—An H II region model for H92α line assuming $T_e = 5000$ K. (*Top left*)*:* The total optical depth (τ, *solid line*) and geometrical size (l, *dashed line*) of an H II region are plotted as functions of the electron density (n_e) for various values of excitation parameter (U). *Top right:* The line flux density (S_L, *solid line*) and the free-free continuum flux density (S_C, *dashed line*) vs. n_e. *Bottom left:* The line optical depth (τ_L, *solid line*) and continuum optical depth (τ_C, *dashed line*) *vs.* n_e. *Bottom right:* The ratio of line to free-free continuum (S_L/S_C, *solid line*) and the non-LTE factor ($F_{\rm nLTE}$, *dashed line*) vs. n_e.

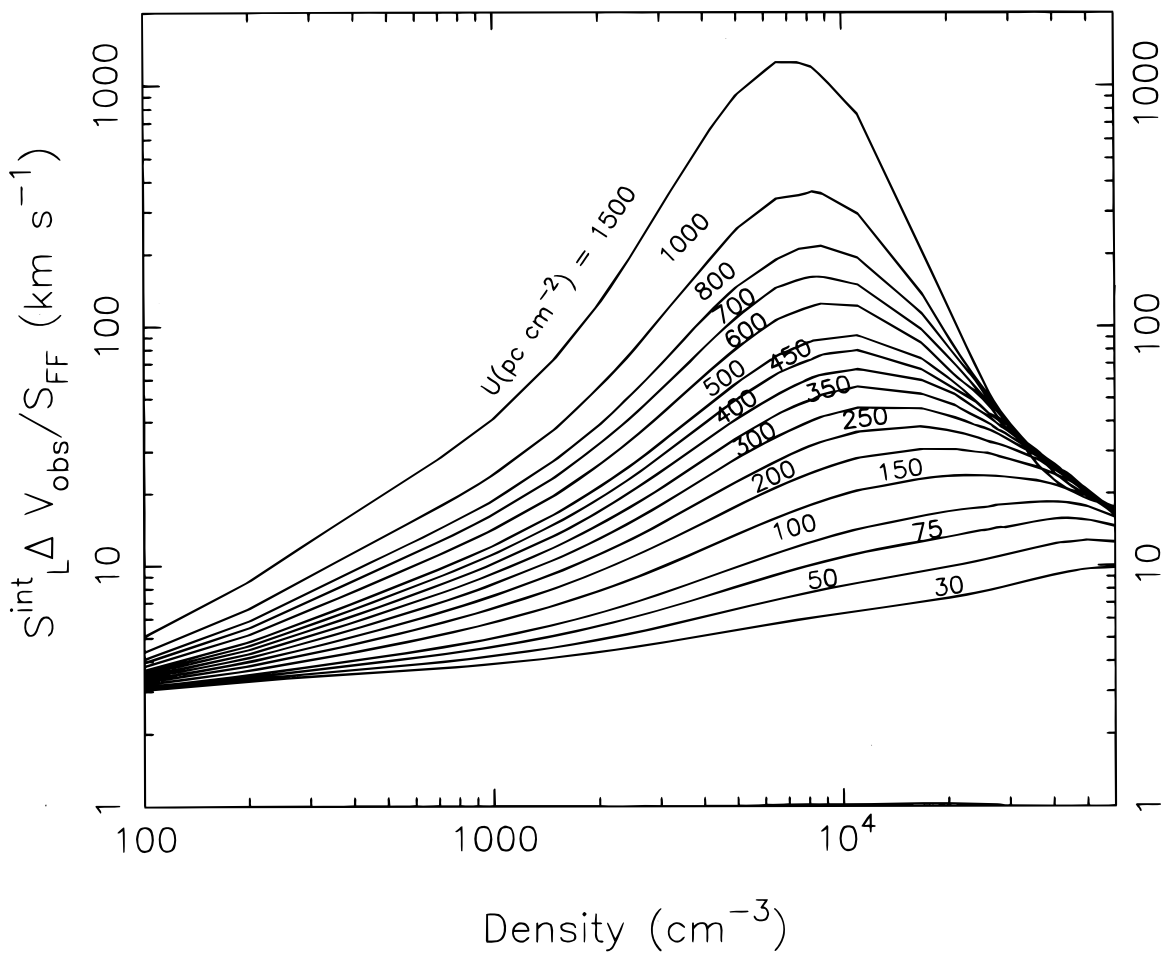

FIG. 15.—A model of a collection H II regions for the H92α line. The ratio of integrated line to continuum ($S_L^{int}\Delta V/S_{FF}$) is plotted as a function of electron density (n_e) for various excitation parameters from 30 to 1500 pc cm^{-2}. The lowest limit for U given here corresponds to a single ZAMS O9 star.

or

$$N\left(\frac{U}{100\ \mathrm{pc\ cm^{-3}}}\right)^3 = 0.063\left(\frac{S_{FF}}{\mathrm{mJy}}\right)D_{\mathrm{Mpc}}^2\,\alpha^{-1}(\nu,\ T_e)T_e^{0.35}\left(\frac{\tau_C}{1-e^{-\tau_C}}\right)\nu_{\mathrm{GHz}}^{0.1}\,. \tag{A11}$$

Both S_{FF} and τ_C, in principle, can be determined from multiwavelength observations. Often, we only observe the continuum flux density S_C^{obs} at a single wavelength, which is the sum of both the radio nonthermal and thermal free-free radiation. In starburst nuclei, the global radio nonthermal and free-free luminosities can be approximately obtained by a simple model with only one free parameter—the average formation rate of massive stars (SFR; $M > 5M_\odot$), which is determined by assuming the extended initial mass function (IMF; $\psi(M) \propto M^{-5/2}$) see Condon 1992). Thus the ratio of free-free to total continuum (S_C) flux densities within a nuclear RRL emission region is approximately

$$\frac{S_{FF}}{S_C} \approx \frac{1}{9.6\nu_{\mathrm{GHz}}^{\alpha+0.1}f(\tau_C)+1}\,, \tag{A12}$$

where α is the nonthermal spectral index ($S \propto \nu^\alpha$) and $f(\tau_C) = \tau_C/(1-e^{-\tau_C})$ is a function of optical depth. At a sufficiently high frequency, the H II regions become optically thin ($\tau_C \ll 1$) and $f(\tau_C)$ in equation (A12) is ~ 1. For large optical depths, $f(\tau_C) \approx \tau_C$. For a given T_e and $S_{FF} \approx (S_{FF}/S_C)S_C^{\mathrm{obs}}$, the possible values for both U and N must be chosen so as to satisfy equation (A11). In addition, since the line width due to a single H II region ($\Delta V_{\mathrm{H\,II}}$) is much smaller than the observed line width (ΔV_{obs}), a minimum number of H II regions with different velocities must exist inside every beam area within the line-emitting region. Thus, the number of H II regions must exceed N_{min} (AZGV):

$$N_{\mathrm{min}} = \frac{\Delta V_{\mathrm{obs}}}{\Delta V_{\mathrm{H\,II}}} \times \frac{\Omega_L}{\Omega_B}\,. \tag{A13}$$

Substituting equation (A13) into equation (A11), we obtain a maximum value for U corresponding to N_{min}; i.e., the excitation parameter for a single H II region must not be greater than U_{upper}, given by

$$\left(\frac{U_{\mathrm{upper}}}{100\ \mathrm{pc\ cm^{-2}}}\right) = 0.33\left(\frac{S_{FF}}{\mathrm{mJy}}\right)^{1/3} D_{\mathrm{Mpc}}^{2/3}\,T_e^{0.12}\alpha^{-1/3}(\nu,\ T_e)\left(\frac{\Delta V_{\mathrm{H\,II}}}{\Delta V_{\mathrm{obs}}}\right)^{1/3}\left(\frac{\Omega_B}{\Omega_L}\right)^{1/3} f(\tau_C)^{1/3}\nu_{\mathrm{GHz}}^{0.03}\,. \tag{A14}$$

A2.2. *The Ratio of Line to Continuum and Lower Limit to the Excitation Parameter*

The ratio of the integrated line-to-continuum intensity for a line emitting region represents an average property of the H II regions:

$$\frac{S_L^{\rm int}\Delta V_{\rm obs}}{S_{FF}} = \frac{S_{L,\rm H\,II}^{\rm int}\Delta V_{\rm H\,II}}{S_{FF,\rm H\ II}}\,, \tag{A15}$$

where $S_{L,\rm H\,II}^{\rm int}$ and $S_{FF,\rm H\ II}$ are the internal line flux density and the free-free continuum flux density of a single H II region.

For $\tau_C \ll 1$ and $|\tau_L + \tau_C| \ll 1$,

$$\frac{S_L^{\rm int}\,\Delta V_{\rm obs}}{S_{FF}} \approx \Delta V_{\rm H\,II}\,\frac{\tau_L^*}{\tau_C}\,b_n\!\left(1 - \frac{\beta_n\tau_C}{2}\right). \tag{A16}$$

For the optically thick case ($\tau_C \gg 1$ and $|\tau_L + \tau_C| \gg 1$), we have

$$\frac{S_L^{\rm int}\,\Delta V_{\rm obs}}{S_{FF}} \approx \Delta V_{\rm H\,II}\!\left(\frac{b_n + \tau_C/\tau_L^*}{b_n\beta_n + \tau_C/\tau_L^*} - 1\right), \tag{A17}$$

where $\tau_C/\tau_L^* = 2.58\,(T_e/5000\ {\rm K})^{1.15}\Delta V_{\rm H\,II}\,\nu_{\rm GHz}^{-1.1}(1 + Y^+)$, and Y^+ is the abundance of singly ionized helium.

In Figure 15 we plot the line-to-continuum ratio for the H92α line as a function of electron density for different values of the excitation parameter (U). Figure 15 shows that the maximum value for the line-to-continuum ratio is proportional to the value of the excitation parameter (U). Therefore, the observed line-to-continuum ratio ($S_L^{\rm int}\Delta V_{\rm obs}/S_{FF}$) sets a lower limit to the mean excitation parameter (U) of a single H II region in the line emission region.

Finally, combining the discussion in §§ A2.1 and A2.2, a suitable range for the excitation parameter (U) can be determined by observing the line-to-continuum ratio ($S_L^1\Delta V_{\rm obs}/S_{FF}$), the FWHM line width ($V_{\rm obs}$), and the angular size of the emission region (Ω_L). A useful procedure is the following:

1. If we assume the H II regions are optically thin, the free-free continuum flux density (S_{FF}) can be evaluated using (A12). If the line is produced mainly by the internal emission ($S_L^{\rm int} \approx S_L$), we can estimate of $S_L^{\rm int}/S_{FF}$. Using the inferred $S_L^{\rm int}/S_{FF}$, we can determine a lower limit for the excitation parameter ($U_{\rm lower}$) by comparing with the theoretical curves in Figure 15.
2. With the assumption of $\tau_C \ll 1$ or $f(\tau_C) \approx 1$, we can evaluate an upper limit for the excitation parameter $U_{\rm upper}$ using equation (A14).
3. If $U_{\rm lower} > U_{\rm upper}$, then $\tau_C \approx U_{\rm lower}/U_{\rm upper}$ and $f(\tau_C) \approx \tau_C/(1 - e^{-\tau_C})$, and we return to step 2 with the inferred value of τ_C instead of the optically thin assumption.
4. Based on the range of U determined above, the corresponding range of electron density (n_e) can be determined from Figure 15. Therefore, we can deduce the other parameters such as the flux of Lyman continuum photons, total ionized mass, the geometrical size and the continuum optical depth (τ_C) of each H II region. Note that higher angular resolution observations at multiwavelengths can, in principle, give a direct determination of these parameters.

REFERENCES

Anantharamaiah, K. R., & Goss, W. M. 1996, ApJ, 466, L13
Anantharamaiah, K. R., Zhao J.-H., Goss, W. M., & Viallefond, F. 1993, ApJ, 419, 585 (AZGV)
Augarde, R., & Lequeux, J. 1985, A&A, 147, 273
Baan, W. A., & Goss, W. M., 1992, ApJ, 385, 188
Baan, W. A., & Haschick, A. D. 1990, ApJ, 364, 65
Boisse, P., Cassoli, F., & Combes, F. 1987, A&A, 173, 229
Carral, P., Turner, J. L., & Ho, P. T. P. 1990, ApJ, 362, 434
Condon, J. J. 1992, ARA&A, 30, 575
Condon, J. J., Condon, M. A., Gisler, G., & Puschell, J. J. 1982, 252, 102
Cornwell, T. J., Uson, J. M., & Haddad, N. A&A, 258, 583
Ford, H. C., et al. 1994, ApJ, 435, L27
Gehrz, R. O., Sramek, R. A., & Weedman, D. E. 1983, ApJ, 267, 551
Harms, R. J., et al. 1994, ApJ, 435, L35
Haynes, M. P., Giovanelli, R. & Roberts, M. S. 1979, ApJ, 229, 83
Huang, Z. P., Condon, J. J., Yin, Q. F., & Thuan, T. X. 1990, IAU Telegrams, Circ. No. 4988
Larson, R. B., & Tinsley, B. M. 1978, ApJ, 219, 46
Puxley, P. J., Brand, P. W. J. L., Moore, T. J. T., Mountain, C. M., & Nakai, N. 1991, MNRAS, 248, 585
Roelfsema, P. R., & Goss, W. M. 1992, A&A, Rev., 4, 161
Rots, A. H. 1978, AJ, 83, 219
Salem, M., & Brockehurst, M. 1979, ApJS, 39, 633
Sanders, D. B., Scoville, N., & Soifer, B. T. 1991, ApJ, 370, 158
Sargent, A. I., & Scoville, N. 1991, ApJ, 366, L1
Seaquist, E. R., & Bell, M. B. 1977, A&A, 60, L1
Seaquist, E. R., Kerton, C. R., & Bell, M. B. 1994, ApJ, 492, 612
Shaver, P. A., Churchwell, E., & Rots, A. H. 1977, A&A, 55, 435
Telesco, C. M., Decher, R., & Gatley, I. 1985, ApJ, 299, 896
Walmsley, C. M. 1990, A&AS, 82, 201
Zhao J.-H., Anantharamaiah, K. R., Goss, W. M., & Viallefond, F. 1996, ApJ, 472, 54 (ZAGV)